Journal of Electroceramics, 7, 77–87, 2001

Aging of NTC Ceramics in the System Mn-Ni-Fe-O

W.A. GROEN,[1] C. METZMACHER,[1] P. HUPPERTZ[1] & S. SCHUURMAN[2]
[1]*Philips Research Laboratories, Weisshausstrasse 2, D-52066 Aachen, Germany*
[2]*BC Components NV, Avenue Franz Guillaume 70, B-1140 Brussels, Belgium*

Submitted September 28, 1999; Revised July 16, 2001; Accepted July 30, 2001

Abstract. The aging behaviour at 150°C of negative temperature coefficient ceramics in the system Mn-Ni-Fe-O has been investigated. Comparison is made between samples cooled in air and in a controlled atmosphere in which no oxidation can occur. The results show that the aging is dependent on composition and is strongly dependent on oxidation which occurs during cooling in air after sintering of the ceramics. From these results a model has been derived which describes the aging mechanism as a migration of cationic vacancies from the grain boundaries to the bulk. Additionally, cations and cationic vacancies migrate to their thermodynamically favourable site in the spinel structure.

Keywords: NTC ceramics, electrical conductivity, aging, defects, spinels

1. Introduction

Negative temperature coefficient (NTC) ceramics or thermistors are widely used for temperature sensing and compensation. The specific resistivity of these semiconducting ceramics is given by the well known Arrhenius equation: $\rho = \rho_0 \exp(E_a/kT)$, in which ρ is the specific resistivity, E_a is the activation energy for conduction, k is Boltzmann's constant and T is the absolute temperature. In the field of NTC ceramics the activation energy is replaced by the thermal constant, B in K, which is related to: $B = E_a/k$. Furthermore, the specific resistivity at 25°C is normally used: ρ_{25}. The charge carriers have a very low mobility of typically 10^{-5}–10^{-8} cm^2/V s at 25°C and are described by the small polaron model [1, 2]. The conductivity in manganite spinels typically used in NTC thermistors is p-type is reported by Suzuki [3] for spinels in the system Mn-Co-Ni-O, Sasamoto et al. [4] for Mn-Fe-Co-Ni-O spinels, Sheftel et al. [5] for Mn-Cu-Co-O spinels and Gilot et al. [6] and Kshirsagar [7] for Mn-Ni-Cu-O spinels. An exception is $NiMn_2O_4$ which shows n-type conductivity but this is a different system since it is highly oxidized [8]. This is in agreement with the results form Larson et al. [9] who report that the conductivity changes from p-type for Ni-Mn-O spinels to n-type for very high amounts of Ni.

A main problem with these materials is aging. There is a drift in resistivity with time which occurs after an annealing at elevated temperatures, i.e. 150°C. In this paper the aging of NTC ceramics in the system Mn-Ni-Fe-O has been investigated. The problem for Fe-containing ceramics is that the aging is much larger than for ceramics with only Mn and Ni. Additionally, the aging properties depend on the amount of Fe. In general, an increase in the resistance, R and the thermal constant, B, is observed. The change of the resistance value ($\Delta R/R_{t=0}$) at 25°C after 1000 h at 150°C can be higher than 20% depending on the composition.

Almost all NTC ceramics crystallize in the spinel structure which can be described by the formula AB_2O_4. In this structure there are two sites available for the cations: a tetrahedral site, A-site, and an octahedral site, B-site. A lot of results on how the cations are distributed over the sites have been published but only some rough guidelines can be given. Mn^{3+} will occupy predominantly the B-site while Mn^{2+} will be on the A-site and almost all Ni^{2+} will go to the B-site [10]. The distribution of the cations depends on the sintering temperature and on the cooling procedure after sintering. For the cubic spinel $(Mn_vNi_{1-v})[Mn_{2-v}Ni_v]O_4$ the inversion parameter v changes from 0.74 when the sample is quenched from high temperature to $v = 0.93$ when the sample is slowly cooled [11]. This is generally

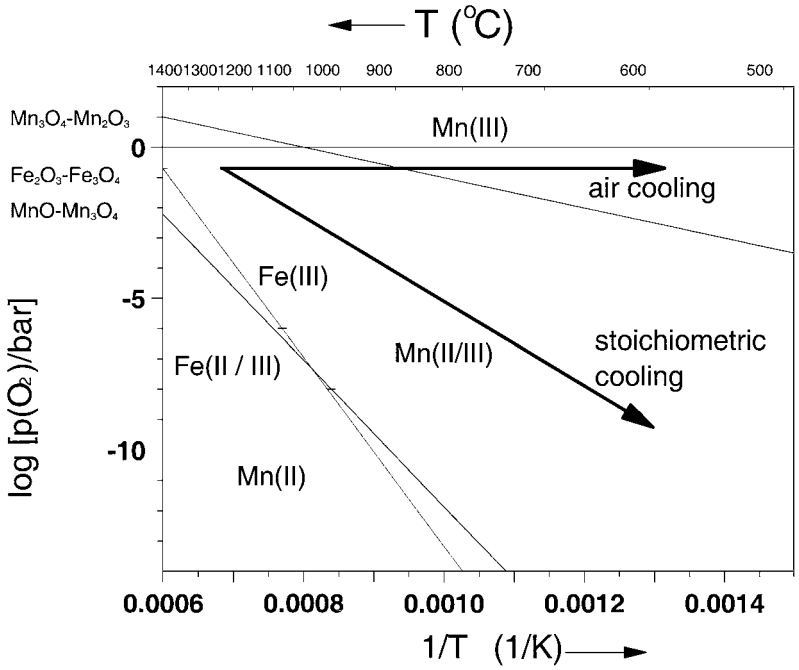

Fig. 1. Stability diagram of the binary oxides of Mn and Fe in equilibrium with oxygen.

found in spinels: at high temperatures the entropy favours a more random distribution of the cations over the different sites. Upon cooling the ordering of the cations to the A- and B-sites occurs. This process should be strongly dependent on the cooling rate.

For the distribution of the Fe-ions the situation is more complicated. An interesting study on the distribution and valency of Fe in the system $Mn_{3-x}Fe_xO_4$ has been reported by Battault et al. [11]. The valency of Fe in this system (air fired samples) is 3+. Up to $Fe = 0.6$ the iron occupies equally A- and B-sites. For higher Fe contents approximately 0.3 Fe goes to the A-site while the rest of the Fe goes to the B-site. A similar distribution was observed for the system $Mn_{2.4-x}Ni_{0.6}Fe_xO_4$ [12].

The NTC ceramics based on spinels in the systems Ni-Mn-Fe-Co-Cu-O are typically sintered at temperatures between 1000 and 1300°C depending on the composition. Normally, the sintering and also the cooling atmosphere is air and as a result the ceramics will oxidize during cooling. This can be best visualized by the phase diagram as presented in Fig. 1. In this diagram the thermodynamic stability of the binary Mn-O and Fe-O oxides is presented [13–15]. It shows which binary oxide is stable at a certain temperature and partial oxygen pressure. The oxidation which happens when a sample is cooled down in air is shown by the horizontal arrow. For instance if Mn_3O_4 is sintered at 1250°C in air ($\log(pO_2) = -0.7$) and slowly cooled in air, it is expected to transform to Mn_2O_3 due to oxidation. To prevent oxidation during cooling, it is possible to use a controlled atmosphere, the so-called "stoichiometric cooling". In this case the amount of oxygen is controlled in a way so that nominally no oxidation (or reduction) occurs. During "stoichiometric cooling" the partial oxygen pressure is regulated as described by Morineau et al. [16]. This process of cooling is schematically presented in Fig. 1 by an arrow. The slope of the arrow represents the value with the mean for the lines Mn_2O_3-Mn_3O_4 and Fe_2O_3-Fe_3O_4 [15].

The diagram as shown in Fig. 1 is only valid for binary compounds which are in equilibrium with the atmosphere. It should be noted that for mixed Mn-Ni-Fe-oxides the diagram is more complicated. The kinetics of the oxidation reactions are not taken into account.

The oxidation reaction for $Ni_{0.5}Mn_{2.5}O_4$ can be described by the following reaction:

$$Ni_{0.5}Mn_{2.5}O_4 + 1/2x\ O_2 \leftrightharpoons Ni_{0.5}Mn_{2.5}V_{0.75x}O_{4+x}$$

in which V is a cationic vacancy. For simplicity we write in the formulas an excess of oxygen: $4 + x$. In

fact, there is little space for interstitial oxygen in this kind of lattice since it is a cubic close packing of oxygen ions. Thus the whole formula should be multiplied by the factor $4/(4+x)$.

Another way of writing this is the Kröger–Vink notation [17]:

$$1/2O_2 \leftrightharpoons O_O^* + 1/4V_A'' + 1/2V_B''' + 2p^\bullet$$

The formed vacancies are distributed over the A- and B-sites. The formal valency for the A-site is 2 and for the B-site is 3. Furthermore, it can clearly be seen that two charge carriers are created per oxygen ion.

Thus, oxidation results in the formation of cationic vacancies at A- and B-sites. Now a redistribution may occur whether these vacancies prefer A- or B-sites. It can be argued that at high temperatures these will be distributed randomly over the lattice as discussed for $NiMn_2O_4$. At lower temperatures the vacancies will be distributed in such a way that the overall energy is minimized. It is known that γ-Fe_2O_3, γ-Mn_2O_3, γ-Al_2O_3 and γ-Cr_2O_3 can crystallize in a defect spinel structure, the so-called gamma phases. Sinha & Sinha [18] have shown that the cationic vacancies are predominantly present at B-sites so these compounds can be described using conventional terminology as $M^{3+}[M^{3+}_{5/3}V_{1/3}]O_4$. So in fact, this is a simple spinel structure with cationic vacancies on the B-site.

Gillot et al. [19] report for an oxidized manganese zinc ferrite also a defect spinel with cationic vacancies on the B-site. For the spinel magnetite, Fe_3O_4, experimental [20] and theoretical [21] evidence show that the cationic vacancies prefer the B-sites. So it may be concluded that the cationic vacancies show a preference for the octahedral site positions in general.

Note, however, that the existance of oxygen vacancies are also reported in the $MgIn_2O_4$ [22] and Li-Mn-O spinels [23].

A number of models have been reported to explain the aging phenonema. Zurbruchen and Case [24] conclude that besides contact degradation, the degree of inversion (the distribution of the cations between tetrahedral and octahedral sites in the spinel) changes upon aging. This is observed from changes in the crystal structure. Feltz [25] reports two models for aging of NTC ceramics: the first is an oxygen uptake or release, the second one is also a redistribution of the cations over the sublattices. Investigations on $Mn_{3-x}Fe_xO_4$ ($x = 0.58$ and 1.05) by means of Mössbauer spectroscopy before and after aging have shown that a migration of Fe^{3+} occurs from the A-site to the B-site [26]. In general it was observed that oxidation results in an increase of aging. However, it cannot be stated that an oxidized ceramic will show fast aging. In the case of $Mn_{3-x}Ni_xO_4$, which has been extremely slowly cooled to room temperature, 6°C/h, no aging was observed [27]. In this case, the heat treatment which is done for the curing of the electrode paste is reported to induce structural and microstructural changes which results in aging.

Recently we reported an investigation of the aging in the series $Mn_{2.46-x}Ni_{0.54}Fe_xO_4$ with $x = 0.75$ and 1.05 [28] by magnetic permeability measurements for samples which are cooled in air after sintering and samples which are stoichiometrically cooled with respect to oxygen content. These experiments showed that the cationic vacancies which are formed because of oxidation during cooling in air are not homogeneously distributed over the ceramics. A grain boundary region with a high concentration of cationic vacancies was assumed which vanishes after aging. So during aging, cationic vacancies migrate to the bulk which results in a homogeneous distribution of cationic vacancies in the ceramic.

2. Experimental

Samples have been prepared from mixtures of Mn_2O_3, NiO and Fe_2O_3 in the appropriate ratios. These powders have been ball-milled on a roll bank and calcined at 800°C for two hours. The calcined powders have been milled again and thereafter have been granulated using polyvinyl-alcohol. Pellets with a diameter of 5.25 mm and a thickness of 2.5 mm were pressed and sintered as follows: 10°C/min to 1250°C → 1 h at 1250°C → 10°C/min to 25°C. The first series has been sintered in air and subsequently cooled in air. The second series of pills were sintered in air and cooled using a controlled atmosphere to avoid oxidation of the ceramics in order to keep the oxygen content constant. The set-up used for these experiments has been described by Verweij et al. [29]. For the electrical measurements, two types of metallization were used: screen printing and vacuum metallization. The resistance value of the samples (15 pieces) was measured in an oil bath at 25°C and 85°C by a two probe technique. The average values of R and B and the standard deviations are calculated. After measurement, they were washed in ethanol and

placed in an oven at 150°C in air. After specified times they are measured again and the shifts $\Delta R/R$ and $\Delta B/B$ were calculated. These are defined as the change in resistance and B value after the aging test, e.g.:

$$\Delta R/R = [R_{25}(t = 1000\text{ h}) - R_{25}(t = 0\text{ h})]/R_{25}(t = 0\text{ h})$$

in which $R_{25}(t = 0$ h) is the resistivity at 25°C before the aging test and $R_{25}(t = 1000$ h) is the resistivity at 25°C after 1000 h aging at 150°C in air.

Complex impedance measurements have been performed using an EG&G Instruments Potentiosat/Galvanostat Model 283 in the frequency range 1 MHz to 1 mHz.

The sign of the Seebeck voltage has been determined by cooling or heating one end of a sintered bar of $2 \times 2 \times 15$ mm^3 (see ref. [9]) and measuring the polarity of the cold end. X-ray diffraction measurements were made with a Philips PW1700 diffractometer using monochromatized Cu Kα radiation. Scanning electron microscopy (SEM) investigations of carbon coated samples have been performed with an acceleration voltage of 10 kV in a Philips XL30 FEG SEM equipped with an EDAX energy-dispersive X-ray analysis system (EDX). The used signals have been secondary electrons (SE) for morphological studies, surface topography and information about porosity as well as characteristic X-rays for elemental mapping and spectroscopy in order to identify potential secondary phases or chemical inhomogenities.

3. Results

3.1. The System $Mn_{2.46-x}Ni_{0.54}Fe_xO_4$

In the first series of experiments, the Fe quantity (x) in the spinel $Mn_{2.46-x}Ni_{0.54}Fe_xO_4$ was varied from 0 to 1.2 with a constant nickel content of Ni = 0.54. Samples have been sintered in air and cooled in air as described in the experimental section. X-ray diffraction on sintered samples showed that all samples with $x > 0$ are single phase and crystallize in a cubic spinel structure. The unit-cell parameters decrease from 845.0 pm for $x = 0.2$ with increasing Fe content to 842.5 pm for $x = 1.2$. The sample without Fe ($x = 0$) crystallizes in a tetragonal crystal structure. The density of the ceramics is higher than 99% of the theoretical density.

The SEM investigations reveal for all samples in this work a homogeneous microstructure without any secondary phases detectable by EDX. From Fig. 2 it can be concluded that an averaged grain size of approximately 3.5 μm and low porosity are typical for the ceramics. No difference between oxidized and stoichiometrically cooled samples has been observed and the microstructure in the range of the interesting compositions appears to be independent of the Ni or Fe amount.

Electrical contacts were made by means of screen printing. The electrical resistivities have been measured at 25 and 85°C. Figure 3 shows R_{25}, the specific resistivity at 25°C, and calculated $B_{25/85}$ values ($B_{25/85} = 1779.7\ \ln(R_{25}/R_{85})$) as a function of x, the Fe content. A slow increase of R_{25} with the Fe content is observed up to $x = 0.7$. For higher iron contents

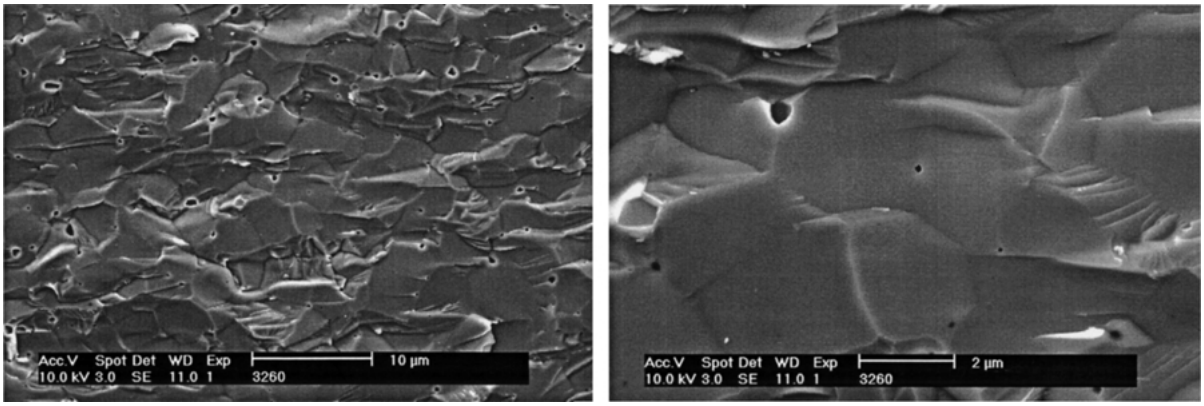

Fig. 2. SE images at two magnifications of a freshly broken surface area of $Mn_{2.46-x}Ni_{0.54}Fe_xO_4$ cooled in air with $x = 1.05$.

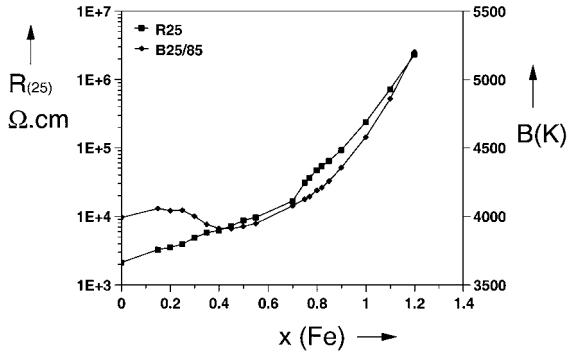

Fig. 3. Specific resistivity and B value for the system $Mn_{2.46-x}\ Ni_{0.54}\ Fe_xO_4$ as a function of the iron content, x.

the increase is more rapidly. The B value slightly decreases with increasing iron content up to Fe = 0.4, for higher iron contents a steady increase of the B value is observed.

After the measurements, the samples were placed in an oven at 150°C in air for the aging test. They were measured again after different aging times (up to 1000 h). The shifts of the specific resistivity, $\Delta R/R$ as a function of time for three samples with a different iron content are presented in Fig. 4.

The R_{25}-value is observed to increase with time. Also the rate of aging is higher for the first 250 h. However, no equilibrium is reached even after 1000 h, the R value continues to increase with time. The shifts in R_{25} are very dependent on the Fe content, except for the samples without Fe which show no aging after 1000 h at 150°C. In Fig. 5 the change in resistivity, $\Delta R/R$ and $\Delta B/B$ after 1000 h at 150°C is shown as a function of the Fe content.

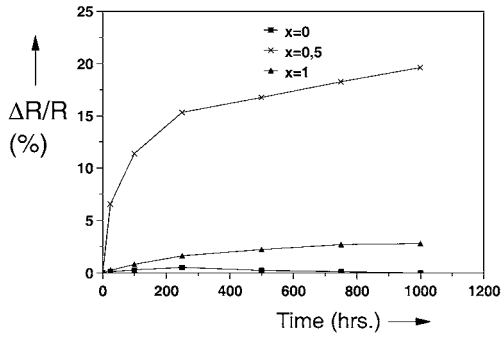

Fig. 4. Relative change in resistance after aging at 150°C for three samples air cooled samples of $Mn_{2.46-x}\ Ni_{0.54}\ Fe_xO_4$ with $x = 0$, 0.5 and 1.

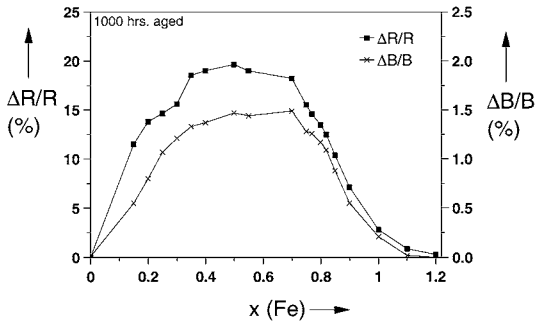

Fig. 5. Relative change in specific resistivity and B-value after 1000 h aging at 150°C as a function of the Fe content, x (air cooled samples).

The curves of $\Delta R/R$ and $\Delta B/B$ both present a maximum value for approximately $x = 0.5$. Furthermore, the values of the shifts in R_{25} are as high as 20% after 1000 h aging at 150°C and aging always results in a positive drift of R_{25} and $B_{25/85}$. Each sample has been analysed by X-ray diffraction before and after aging, but no significant change in the unit cell parameters could be observed.

3.2. *The System* $Mn_{2.25-y}Fe_{0.75}Ni_yO_4$

As shown above, the iron content has a large influence on the aging properties. To investigate the influence of the Ni content on aging, a series of samples were prepared with a constant Fe content of 0.75 and a varying Ni content. The value of Fe = 0.75 was chosen because this composition shows a relatively high degree of aging. X-ray diffraction on sintered ceramics show that samples with a high Ni content are sensitive for demixing of the spinel at high temperature which results in the formation of NiO as a second phase. For nominal nickel contents higher than 0.7 it has been observed by XRD that NiO is indeed present as a second phase in the specimens. Due to the low cation mobility of Ni, the second phase is maintained during cooling in air. In Fig. 6, the R_{25} and $B_{25/85}$ values are presented as a function of y, the Ni content. An increase of the Ni content results in a decrease of the specific electrical resistivity and the B-value. The results of the aging test after 100 h at 150°C are presented in Fig. 7. It shows that $\Delta R/R$ and $\Delta B/B$ are a strong function of the nickel content. For low Ni contents a relatively high aging is observed. However, for Ni = 0.7 and higher almost no aging is observed.

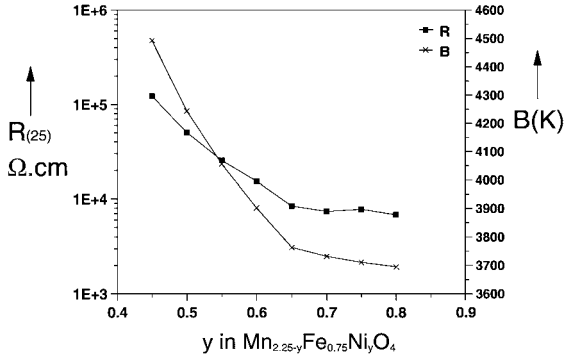

Fig. 6. Specific resistivity and B-value for $Mn_{2.25-y}\,Fe_{0.75}\,Ni_yO_4$ cooled in air as a function of the nickel content, y.

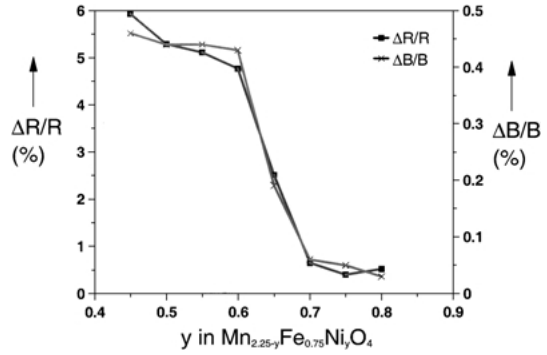

Fig. 7. Relative change in resistance and B-value after 100 h aging at 150°C for $Mn_{2.25-y}\,Fe_{0.75}\,Ni_yO_4$ cooled in air as a function of the nickel content, y.

3.3. Stoichiometric Cooling

As discussed in the introduction, cooling in air after sintering is expected to result in the oxidation of the ceramics. To investigate the effect of this oxidation, a series of experiments has been performed with $Mn_{2.46-x}Ni_{0.54}Fe_xO_4$ in which the ceramics were cooled stoichiometrically with respect to oxygen content after sintering. Electrical contacts have been made by vacuum metallization to prevent oxidation which might occur during the curing of the conductive paste in case of screen printing. The measured specific resistivities and $B_{25/85}$ values for these ceramics are slightly higher than those of the air cooled samples, which are discussed in Section 3.1. After the measurements, the samples were aged in an oven at 150°C in air. After 1000 h the samples were measured again and

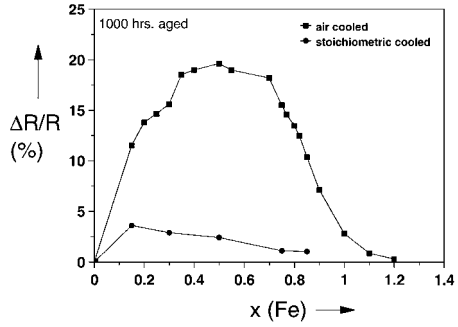

Fig. 8. Relative change in specific resistivity, R_{25}, after 1000 h aging at 150°C as a function of the Fe content for $Mn_{2.46-x}\,Ni_{0.54}\,Fe_xO_4$ cooled stoichiometrically. The data for air cooled samples are given for comparison.

the resulting shift in R_{25} and $B_{25/85}$ was calculated. The shift in R_{25} as a function of the iron content, x, in the samples is presented in Fig. 8. The values for air cooled samples are given for comparison. It is shown that the stoichiometrically cooled samples show much less aging than the air cooled samples. The shifts in $\Delta B/B$ are typically smaller than 0.5%. These results clearly demonstrate that the oxidation which occurs during cooling down in air has a large impact on the aging behavior of the ceramics. Furthermore, the stability is less dependent on the composition.

3.4. Complex Impedance Spectroscopy and Sign of Seebeck Coefficient

To insure that the differences with respect to aging at 150°C in air observed between air cooled and stoichiometrically cooled samples of $Mn_{2.46-x}Ni_{0.54}Fe_xO_4$ are bulk effects rather than electrode and grain boundary effects, complex impedance measurements were made at 25°C. Samples of air cooled $Mn_{2.46-x}Ni_{0.54}Fe_xO_4$: $x = 0$, 0.5, 1.0 with screen printed contacts and "stoichiometrically cooled" $Mn_{2.46-x}Ni_{0.54}Fe_xO_4 : x = 0$, 0.5, 1.0 with electrical contacts prepared by vacuum metallization were measured before and after the aging test at 150°C in air. In all samples, just one semicircle was observed for which the calculated capacitance confirmed this semicircle to be related to the bulk resistance. No electrode effects or grain boundary resistances are observed.

The sign of the Seebeck coefficient was measured for air cooled $Mn_{2.46-x}Ni_{0.54}Fe_xO_4 : x = 0$, 0.25, 0.5,

0.75, 1.0 and 1.2. Electrical contacts were made by screen printing. All six samples showed a positive Seebeck voltage indicating p-type conductivity.

4. Discussion

4.1. Oxidation

From the experiments performed, it is clear that there are large differences with respect to aging at 150°C in air between samples of $Mn_{2.46-x}Ni_{0.54}Fe_xO_4$ cooled in air and those cooled stoichiometrically. The oxidation which occurs during air cooling after sintering has a large influence on aging. Therefore, before discussing the aging behavior, a description of what happens during oxidation is necessary. As discussed in the introduction, the incorporation of one oxygen atom results in the formation of two electron-holes and 3/4 cationic vacancies. As a result of the increased hole concentration, one might expect that the specific resistivity decreases since the material is a p-type conductor. However, in nearly all cases the opposite is observed (especially for low carrier- or low Ni-concentrations). This implies that the concentration of charge carriers does not only dominate the resistivity but that the mobility of the charge carriers is also of importance.

As an example, data for the system $Mn_{3-x}Ni_xO_4$ are presented in Fig. 9 [30] showing the specific resistivity of quenched and air cooled samples as a function of x. For the quenched samples, there is only a very weak dependence of the resistivity on the nickel content. The more the samples are oxidized, the higher the specific resistivity for the low Ni content samples. As discussed before, oxidation results also in the formation of cationic vacancies. The conduction in NTC resistors

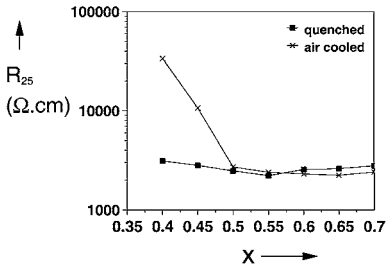

Fig. 9. Specific resistivity for samples of $Mn_{3-x}Ni_xO_4$ versus nickel content: quenched samples, slowly cooled sampled with contacts made by evaporation.

is generally described by electron or hole hopping over B-sites in the spinel lattice [1, 2, 9]. Support for this comes from the distances between the different sites. For a cubic spinel with $a_0 = 84.5$ pm these distances are calculated as: B–B = 29.9 pm, A–B = 35.0 pm and A–A = 36.6 pm. So when there is an empty B-site (a metal vacancy on the B-site) in the lattice one can argue that this leads to an increase in resistivity. The concentration of metal vacancies in spinels can be high as is shown for γ-Mn_2O_3 [18] which can be described as $M^{3+}[M^{3+}_{5/3}V_{1/3}]O_4$. Furthermore, low temperature (up to 425°C) oxidation of Haussmannite, Mn_3O_4, results in the formation of a defect spinel of formula $Mn_2O_{2.78}$ ($= Mn_{2.88}O_4$) [31].

The other interesting result deduced from Fig. 9 is that on the Ni-rich side, oxidation during cooling in air, seems to have no (or a very small) effect on the specific resistivity. From the results discussed above, a tentative conclusion may be drawn that in these samples oxidation does not result in the formation of cationic vacancies. Therefore these samples probably have oxygen vacancies at high temperatures. When such a sample is oxidized the oxygen vacancies are filled at first:

$$V_O^{\bullet\bullet} + 1/2O_2 \leftrightharpoons O_O^* + 2p^{\bullet}$$

As a result of this, the charge carrier concentration increases and the specific resistivity decreases as observed (see Fig. 9 for the samples with a high Ni content). The oxygen vacancies are expected to have a small influence on the mobility of the charge carriers in contradiction to cationic vacancies as discussed above since they are not directly involved in the conduction mechanism.

4.2. Phase Diagram

In general, it can be stated that the stoichiometry of a metal oxide depends on the partial oxygen pressures when it is in thermal equilibrium. When the partial oxygen pressure is too high, at first oxidation occurs which results in the formation of cationic vacancies as discussed in the previous section. With increasing oxygen partial pressure, a certain limit is reached at which decomposition occurs. In the case of NiMn-oxides, at this point, the spinel is decomposed to Mn_2O_3 and a nickel rich cubic spinel. The same result has been reported by Larson et al. [9].

For low oxygen partial pressures, reduction of the compound occurs. Now two things may happen: the

formation of oxygen vacancies as described by:

$$O_O^* \leftrightharpoons 2e' + V_O^{\bullet\bullet} + 1/2O_2 \quad \text{or}$$
$$O_O^* + 2p^{\bullet} \leftrightharpoons V_O^{\bullet\bullet} + 1/2O_2.$$

This results in the formation of two electrons and an oxygen vacancy. Another reaction which may occur is the formation of interstitial cations:

$$Mn_3O_4 \leftrightharpoons Mn_i^{\bullet\bullet(\text{tetrahedral})} + 2Mn_i^{\bullet\bullet\bullet(\text{octahedral})} + 8e' + 2O_2.$$

The net result of both reactions is the same, therefore only the first one is considered. For lower oxygen partial pressures, decomposition of the spinel is observed which leads in the case of a NiMn-oxide to the formation of NiO and nickel poor spinel. Again similar results are reported by Larson et al. [9].

Note that reduction and oxidation are very strongly dependent on the temperature, as has already been discussed (see Introduction and Fig. 1). Therefore an increase of temperature has a similar effect as a decrease of the oxygen partial pressure and vice-versa. These results can be presented schematically in a phase diagram as shown in Fig. 10. The dashed line in the center of the diagram represents an ideal stoichiometric spinel with "no" vacancies. Below this line, oxygen vacancies are present and above this line, cationic vacancies are present. When ceramics are cooled under conditions represented by the lower side of the phase diagram (below the dashed line), oxidation does not result in formation of cationic vacancies but rather in

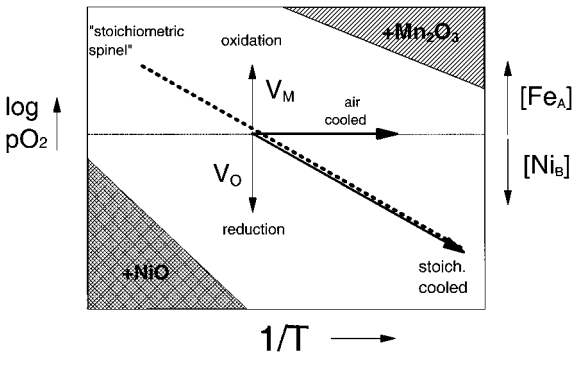

Fig. 10. Phase diagram for NTC ceramics consisting of manganite spinels doped with nickel and/or iron. In this diagram the relations are shown between composition and reduction or oxidation.

the filling of oxygen vacancies. As discussed in the previous section, the mobility of the charge carriers is of importance. Therefore, since the conduction is by a hopping process over B-sites, cationic vacancies at the B-site will have a large impact, while oxygen vacancies will not. This is in good agreement with the observed data for the system $Mn_{3-x}Ni_xO_4$ as presented in Fig. 9.

The introduction of Ni^{2+} will "reduce" the ceramic because of the formation of oxygen vacancies. As discussed in the introduction, the Ni will predominantly occupy the B-site in the spinel:

$$6Mn_B^* + 3O_O^* + 6NiO \leftrightharpoons 6Ni_B' + 2Mn_3O_4 + 3V_O^{\bullet\bullet} + 1/2O_2.$$

The same happens when the ceramics are reduced. As a result, the composition represented in the phase diagram of Fig. 10 will move to the bottom.

The introduction of Fe^{3+} on the B-site in a spinel has no influence on the charge balance since it replaces a Mn^{3+} ion. However, when the Fe^{3+} ion occupies the A-site it replaces a Mn^{2+} ion. As a result, a cationic vacancy is created:

$$3Mn_A^* + 1/2O_2 + Fe_2O_3 \leftrightharpoons 2Fe_A^{\bullet} + Mn_3O_4 + V_A''$$

The same happens if the ceramics are oxidized. As a result, the composition represented in the phase diagram will move up and consequently will become more sensitive to oxidation. Note that the distribution of the iron ions over the sublattices is already discussed in the introduction.

These results can be verified by the experiments described in Section 3.2 on the system $Mn_{2.25-y}Fe_{0.75}Ni_yO_4$. In the system $Mn_{3-y}Ni_yO_4$ cationic vacancies are formed for values of y lower than approximately 0.5 (see Fig. 9). In $Mn_{2.25-y}Fe_{0.75}Ni_yO_4$: 0.29 Fe is located on A-sites [11, 12]. Thus for $Ni = 0.5$ this compound will be sensitive to oxidation during cooling and will not be stable in the aging tests as observed. However, when the nickel content is increased to values higher than 0.7 the stability is good again indicating that no cationic vacancies are present. Note that it was expected that the stability would improve at $Ni = 0.79$ $(= 0.5 + 0.29)$, so this is in agreement when taking the relative errors into account. The error may be due to the fact that not all Ni is present at the B-sites which is assumed.

4.3. Aging

Oxidation of $Ni_{0.5}Mn_{2.5}O_4$ results in a spinel with cationic vacancies which are not homogeneously distributed but are enriched at the grain boundaries. However, this compound does not show a high aging compared to the Fe-substituted samples. Therefore, the existance of cationic vacancies is not only responsible for the aging phenomena. As discussed before, the introduction of Fe does increase the aging considerably. From Mössbauer investigations by Battault et al. [26] it is clear that a reordering of Fe occurs over the sites during aging. This reordering of the cations is probably due to the fact that during cooling after sintering, the cations do not order completely in their thermodynamically stable site. Consequently, at the elevated temperatures during aging, a slow reordering of the cations might happen. That such a process is not unlikely to occur at 150°C, it is of importance to note that Brabers [32] noticed a cation exchange between the octahedral and tetrahedral sublattices at 200°C in the system $Mn_xFe_{3-x}O_4$. The speed of cation reordering is most probably dependent on the amount of cation vacancies available. If there are cation vacancies available there will be a neighboring site available for a cation to hop/diffuse to. As an example, the site swapping between an Fe at an A-site and an Mn at an B-site can be described as follows:

$$\mathrm{Fe_A} + \mathrm{V_B} \rightarrow \mathrm{Fe_B} + \mathrm{V_A} \quad \text{followed by}$$
$$\mathrm{Mn_B} + \mathrm{V_A} \rightarrow \mathrm{Mn_A} + \mathrm{V_B}.$$

It is clear that these reactions do not occur when there are no available cation vacancies. Note that also a diffusion of cation vacancies to the B-sites is expected to occur because the cationic vacancies show a higher preferential energy for the octahedral sites as discussed in the introduction. This is probably the reason why, in almost all cases, an increase of the resistivity is observed upon aging.

Summarizing the results described above and those from the magnetic measurements described in ref. [28] the aging can be described by the following process:

(1) cationic vacancy migration from grain boundary to bulk
(2) cation vacancy assisted migration of cations (also vacancies) to thermodynamically stable site.

As a result of these processes there is an increase of metal vacancies on the B-sites in the spinel inside the grains, which results in an increase of the resistivity since the hole conduction is over the B-sites in these spinels as discussed.

Support for this description of the aging mechanism in NTC ceramics crystallizing in the spinel structure is given by a study on the system $NiAl_2O_4$ [33]. Here a disorder of the cations is induced by a temperature-jump experiment, and the kinetics of the cation exchange are studied from relaxation. Samples with cationic vacancies show a fast exchange while samples with no cationic vacancies show a very slow relaxation. It is concluded from these experiments that the cation exchange mechanism is of vacancy controlled type.

The effect of various heat treatments on aging of NTC ceramics using the model described above can be summarized in Fig. 11.

In case of stoichiometrically cooled or quenched samples there will be no oxidation during cooling. As a result, the cationic vacancy concentration will be low. Therefore it is expected that the stability for the stoichiometrically samples will be good as has been observed. However, for quenched samples the stability is questionable since there will be a strong disordering of the cations.

For air cooled samples there will be an oxidation starting from the grain boundaries which results in the formation of cationic vacancies. At sufficient high temperatures these vacancies can diffuse into the grain but at still lower temperatures the vacancies will be trapped at the grain boundary. The result is a NTC ceramic with a high cationic vacancy concentration and a non-ideal distribution of cations and cationic vacancies, thus the ceramics will be unstable with respect to aging. After prolonged aging the cationic vacancies will be distributed homogeneously over the ceramics. Furthermore, the cations and cationic vacancies migrate to their ideal site. Consequently after the aging test, the ceramics reach a state in which they are stable. One problem which arises from too high aging temperatures is a simultaneous oxidation of the ceramics. In this case the ceramics will never be stable because there is a continuous generation of cationic vacancies at the grain boundaries. At last it is of interest to note that is has been reported that ceramics which are extremely slowly cooled in air are stable with respect to aging if the electrical contacts are made by vacuum metallization [27]. For these ceramics there will be severe oxidation and thus formation of cationic vacancies. But since the cooling rate is very slow there will be time for the cationic vacancies to diffuse into the grains and the

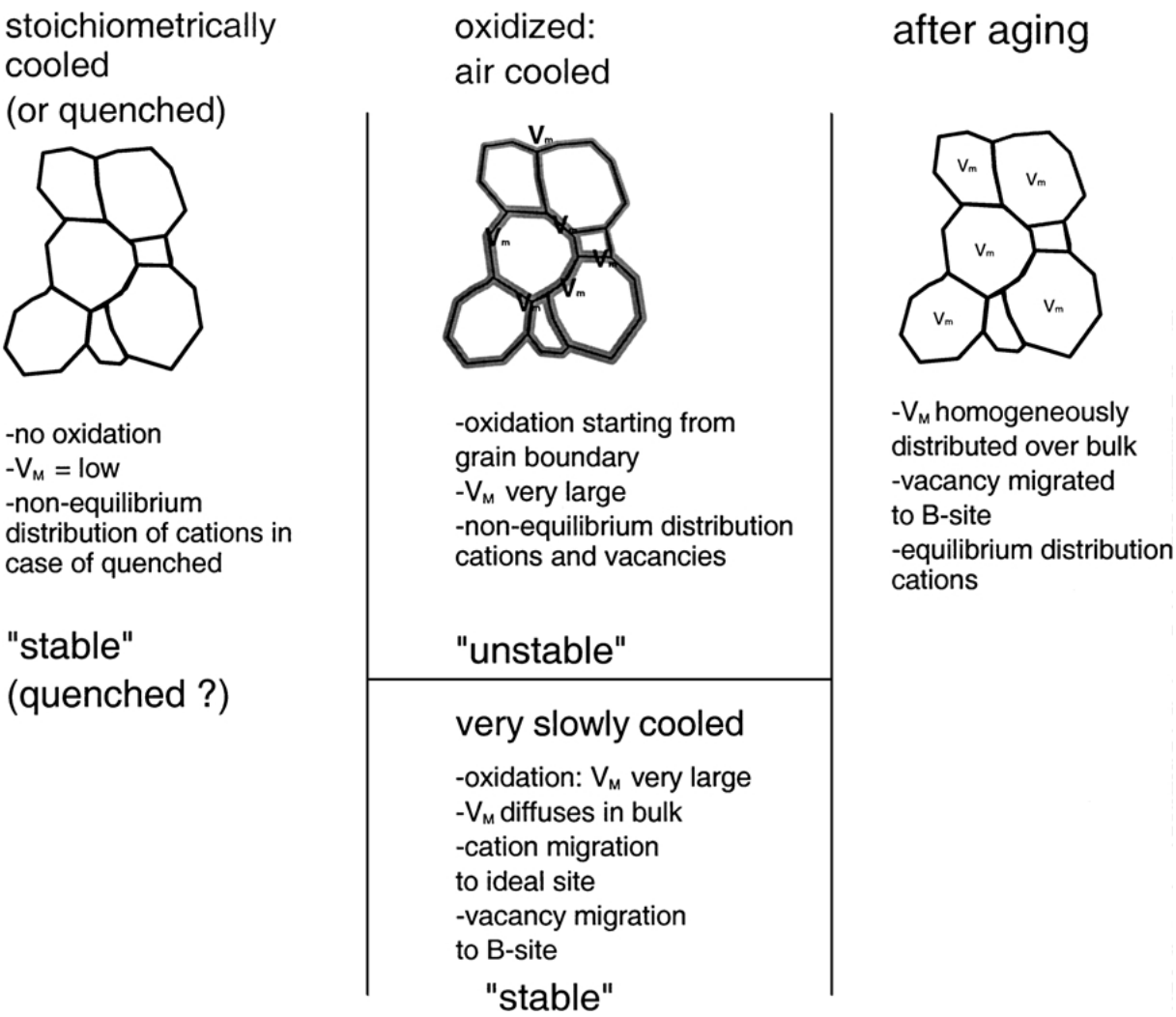

Fig. 11. The impact of various heat treatment on the stability of NTC ceramics.

distribution of cations and vacancies will reach equilibrium. However, when the electrical contact are made by screen printing (and as a consequence are heated for a short time at 850°C for curing) the stability with respect to aging is low [27]. This can be explained because during the short heating cycle a disordering of cations and cationic vacancies will occur.

5. Conclusions

The aging behaviour of NTC ceramics is shown to be strongly dependent on the oxidation which occurs after sintering during cooling down in air. A model has been developed which describes the mechanism of this aging:

(1) cationic vacancy migration from grain boundary to bulk
(2) cation vacancy assisted migration of cations (also vacancies) to thermodynamic stable site occupation.

The model predicts that the specific resistivity is always expected to increase when ceramics are aged. This is in good agreement with experimental observations and cannot be explained by the existing models.

Acknowledgments

We would like to thank K. Albertsen, H.D. Bausen, H. Kohler, J. Merx, K. Herff, C. Borst and V. Sillen for lots of stimulating discussions and experimental work.

References

1. E.J.W. Verweij, P.W. Haaijman, F.C. Romeijn, and C.W. Oosterhout, *Philips. Res. Rep.*, **5**, 173 (1950).
2. E.D. Macklen, *Thermistors* (Electrochemical Publications Ltd., Ayr, Scotland, 1979).
3. M. Suzuki, *J. Phys. Chem. Solids*, **41**, 1253 (1980).
4. T. Sasamoto, T. Meguro, T. Yokoyama, Y. Abe, and M. Torikai, *Key Eng. Mater.*, **53–55**, 101 (1991).
5. I.T. Sheftel, A.I. Zaslavskii, E.V. Kurlina, and G.N. Tekster-Proskuryakova, *Soviet Phys. Solid St.*, **3**, 1979 (1962).
6. B. Gilot, M. Kharroubi, R. Metz, and A. Rousset, *Sol. St. Ionics*, **48**, 93 (1991).
7. S.T. Kshirsagar, *J. Phys. Soc. Jp.*, **27**, 1164 (1969).
8. V.A.M. Brabers and J.C.J.M. Terhell, *Phys. Stat. Sol.* A, **69**, 325 (1982).
9. E.G. Larson, R.J. Arnott, and D.G. Wickham, *J. Phys. Chem. Solids*, **23**, 1771 (1962).
10. B. Boucher, R. Buhl, and M. Perrin, *Acta. Cryst.*, B **25**, 2326 (1969).
11. T. Battault, R. Legros, and A. Rousset, *J. Eur. Ceram. Soc.*, **15**, 1141 (1995).
12. T. Battault, R. Legros, and A. Rousset, *J. Mat. Syn. and Proc.*, **4**, 361 (1996).
13. E.M. Otto, *J. Electrochem. Soc.*, **112**, 367 (1965).
14. L.S. Darken and R.W. Gurry, *J. Am. Chem. Soc.*, **68**, 798 (1946).
15. I. Barin, *Thermochemical Data of Pure Substances* (VCH Verlagsgesellschaft, Weinheim, Germany, 1989).
16. R. Morineau and M. Paulus, *IEEE Trans. on Magnetics*, **11**, 1312 (1975).
17. F.A. Kröger, *The Chemistry of Imperfect Crystals*, 2nd ed. (North Holland Publishing Co., New York, 1973).
18. K.P. Sinha and A.P.B. Sinha, *J. Phys. Chem.*, **61**, 758 (1957).
19. B. Gillot and M. El Guendouzi, *J. Solid. State Chem.*, **106**, 443 (1993).
20. J.M. Daniels and A. Rosencwaig, *J. Phys. Chem. Solids*, **30**, 1561 (1969).
21. G.V. Lewis, C.R.A. Catlow, and A.N. Cormack, *J. Phys. Chem. Solids*, **46**, 1227 (1985).
22. N. Ueda, T. Omata, N. Hikuma, K. Ueda, H. Mizoguchi, H. Hashimoto, and H. Kawazoe, *Appl. Phys. Lett.*, **61**, 1954 (1992).
23. H. Tanji, N. Kurihara, and M. Yoshida, *J. Mat. Sci. Lett.*, **23**, 1673 (1994).
24. J.M. Zurbuchen and D.A. Case, *Proc. 6th Int. Symp. on Temperature its Measurement and Application*, edited by J.F. Schooley, part 2, 889 (1982).
25. A. Feltz, *Proc. Electroceramics IV*, edited by R. Waser, 677 (1994).
26. T. Battault, R. Legros, M. Brieu, J.J. Couderc, L. Bernard, and A. Rousset, *J. Phys. III France*, **7**, 979 (1997).
27. S. Fritsch, J. Sarrias, M. Brieu, J.J. Couderc, J.L. Badour, E. Snoeck, and A. Rousset, *Solid State Ionics*, **109**, 229 (1998).
28. W.A. Groen, V. Zaspalis, and S. Schuurman, *J. Mater. Sci. Let.*, **18**, 1233 (1999).
29. H. Verweij and W.H.M. Bruggink, *J. Phys. Chem. Solids*, **50**, 75 (1989).
30. W.A. Groen, P. Huppertz, S. Schuurman, J. Hertz, and H. Tuller, unpublished.
31. S. Fritsch, J. Sarrias, A. Rousset, and G.U. Kulkarni, *Mater. Res. Bull.*, **33**, 1185 (1998).
32. V.A.M. Brabers, *J. Phys. Chem. Solids*, **32**, 2181 (1971).
33. J. Bäckermann and K.D. Becker, *Z. Phys. Chem.*, **206**, 31 (1998).